

# Interpolation of Sparse High-Dimensional Data

Thomas C. H. Lux · Layne T. Watson ·  
Tyler H. Chang · Yili Hong · Kirk  
Cameron

Received: date / Accepted: date

**Abstract** Increases in the quantity of available data have allowed all fields of science to generate more accurate models of multivariate phenomena. Regression and interpolation become challenging when the dimension of data is large, especially while maintaining tractable computational complexity. Regression is a popular approach to solving approximation problems with high dimension, however there are often advantages to interpolation. This paper presents a novel and insightful error bound for (piecewise) linear interpolation in arbitrary dimension and contrasts the performance of some interpolation techniques with popular regression techniques. Empirical results demonstrate the viability of interpolation for moderately high dimensional approximation problems, and encourage broader application of interpolants to multivariate approximation in science.

**Keywords** approximation · regression · interpolation · high dimension · error bound

## 1 Introduction

Regression and interpolation are problems of considerable importance that find applications across many fields of science. Pollution and air quality analysis [17], energy consumption management [28], and student performance prediction [14, 31] are a few of many interdisciplinary applications of multivariate regression for predictive analysis. As discussed later, these techniques can also be applied to prediction problems related to forest fire risk assessment [13],

---

This work was supported by the National Science Foundation Grant CNS-1565314.

---

Thomas Lux  
Virginia Polytechnic Institute & State University (VPI&SU)  
Blacksburg, VA 24061  
E-mail: tchlux@vt.edu

Parkinson’s patient clinical evaluations [43], local rainfall and weather [45], credit card transactions [37], and high performance computing (HPC) file input/output (I/O) [32].

Regression and interpolation have a considerable theoretical base in one dimension [10]. Splines in particular are well understood as an interpolation technique in one dimension [5], particularly B-splines. Tensor products of B-splines [44] or other basis functions have an unfortunate exponential scaling with increasing dimension. Exponential scaling prohibits tensor products from being reasonably applied beyond three-dimensional data. In order to address this dimensional scaling challenge, C. de Boor and others proposed box splines [6], of which one of the approximation techniques in this work is composed [33].

The theoretical foundation of low dimensional interpolation allows the construction of strong error bounds that are absent from high dimensional problems. This work extends some known results regarding the secant method [18] to construct an interpolation error bound for problems of arbitrary dimension. These error bounds are useful, considering the same cannot be said for regression algorithms in general. The maximum complexity of an interpolant is bounded by the amount of data available, while the maximum complexity of a regressor is bounded by both the amount of data and the chosen parametric form. For this reason, generic uniform bounds are largely unobtainable for regression techniques on arbitrary approximation problems, even when the approximation domain is bounded.

Aside from theoretical motivation for the use of interpolants, there are often computational advantages as well. Interpolants do not have the need for *fitting* data, or minimizing error with respect to model parameters. In applications where the amount of data is large and the relative number of predictions that need to be made for a given collection of data is small, the direct application of an interpolant is much less computationally expensive.

In this work, multivariate interpolation is defined given a closed convex subset  $Y$  of a metrizable topological vector space with metric  $s$ , some function  $f : \mathbb{R}^d \rightarrow Y$  and a set of points  $X = \{x^{(1)}, \dots, x^{(n)}\} \subset \mathbb{R}^d$ , along with associated function values  $f(x^{(i)})$ . The goal is to construct an approximation  $\hat{f} : \mathbb{R}^d \rightarrow Y$  such that  $\hat{f}(x^{(i)}) = f(x^{(i)})$  for all  $i = 1, \dots, n$ . It is often the case that the form of the true underlying function  $f$  is unknown, however it is still desirable to construct an approximation  $\hat{f}$  with small approximation error at  $y \notin X$ . The two metric spaces that will be discussed in this work are the real numbers with metric  $s(x, y) = |x - y|$ , and the set of cumulative distribution functions (CDFs) with the Kolmogorov-Smirnov (KS) statistic [30] as metric.

Multivariate regression is often used when the underlying function is presumed to be stochastic, or stochastic error is introduced in the evaluation of  $f$ . Hence, multivariate regression relaxes the conditions of interpolation by choosing parameters  $P$  defining  $\hat{f}(x; P)$  to minimize the error vector  $(|\hat{f}(x^{(1)}; P) - f(x^{(1)})|, \dots, |\hat{f}(x^{(n)}; P) - f(x^{(n)})|)$  in some norm. The difficult question in

the case of regression is often what parametric form to adopt for any given application.

The most challenging problem when scaling in dimension is that the number of possible interactions between dimensions grows exponentially. Quantifying all possible interactions becomes intractable, and hence beyond three-dimensional data mostly linear models are used. That is not to say nonlinear models are absent, but nonlinearities are often either preconceived or model pairwise interactions between dimensions at most. Even globally nonlinear approximations such as neural networks are constructed from compositions of summed low-interaction functions [12].

Provided the theoretical and practical motivations for exploring interpolants, this work aims to study the empirical performance differences between a set of scalable (moderately) interpolation techniques and a set of common regression techniques. These techniques are applied to a collection of moderately high dimensional problems ( $5 \leq d \leq 30$ ) and the empirical results are discussed.

The remainder of this paper is organized as follows. Sections 2 and 3 present the multivariate models. Section 4 gives the error measuring methodology that is used for collecting empirical results. Section 5 contains the theoretical error bounds for interpolation **as well as an analytic test for demonstration**. Section 6 presents the data sets for empirical approximation analysis and the approximation results for all models on these data sets. Section 7 analyzes and discusses the results, their implications, and their limitations. Finally, Section 8 concludes.

## 2 Multivariate Regression

Multivariate regressors are capable of accurately modeling a complex dependence of a response (in  $Y$ ) on multiple variables (represented as a points in  $\mathbb{R}^d$ ). The approximations to some (unknown) underlying function  $f : \mathbb{R}^d \rightarrow Y$  are chosen to minimize some error measure related to data samples  $f(x^{(i)})$ . For example, least squares regression uses the sum of squared differences between modeled function values and true function values as an error measure. In this section and the next, some techniques are limited to approximating real valued functions ( $Y \subset \mathbb{R}$ ). These techniques can be extended to real vector-valued ranges by repeating the construction for each component of the vector output. Throughout the following,  $x$  denotes a  $d$ -tuple,  $x_i$  the  $i$ th component of  $x$ , and  $x^{(i)}$  the  $i$ th  $d$ -tuple data point. Different symbols are used to represent the approximation function  $\hat{f}$ .

### 2.1 Multivariate Adaptive Regression Splines

This approximation was introduced in [20] and subsequently improved to its current version in [21], called fast multivariate adaptive regression splines (Fast

MARS). In Fast MARS, a least squares fit model is iteratively built by beginning with a single constant valued function and adding two new basis functions at each iteration of the form

$$\begin{aligned} B_{2j-1}(x) &= B_l(x)(x_i - x_i^{(p)})_+, \\ B_{2j}(x) &= B_k(x)(x_i - x_i^{(p)})_-, \end{aligned}$$

where  $j$  is the iteration number,  $1 \leq p \leq n$ , and  $B_l(x)$ ,  $B_k(x)$  are basis functions from the previous iteration,

$$w_+ = \begin{cases} w, & w \geq 0 \\ 0, & w < 0 \end{cases},$$

and  $w_- = (-w)_+$ . After iteratively constructing a model, MARS then iteratively removes basis functions that do not contribute to goodness of fit. In effect, MARS creates a locally component-wise tensor product approximation of the data. The overall computational complexity of Fast MARS is  $\mathcal{O}(ndm^3)$  where  $m$  is the maximum number of underlying basis functions. This paper uses an implementation of Fast MARS [39] with  $m = 200$  throughout all experiments.

## 2.2 Support Vector Regressor

Support vector machines are a common method used in machine learning classification tasks that can be adapted for the purpose of regression [3]. How to build a support vector regressor (SVR) is beyond the scope of this summary, but the resulting functional fit  $p : \mathbb{R}^d \rightarrow \mathbb{R}$  has the form

$$p(x) = \sum_{i=1}^n a_i K(x, x^{(i)}) + b,$$

where  $K$  is the selected kernel function,  $a_i \in \mathbb{R}^n$ ,  $b \in \mathbb{R}$  are coefficients to be solved for simultaneously. The computational complexity of the SVR is  $\mathcal{O}(n^2 dm)$ , with  $m$  being determined by the minimization convergence criterion. This paper uses the scikit-learn SVR [36] with a radial basis function kernel.

## 2.3 Multilayer Perceptron Regressor

The neural network is a well studied and widely used method for both regression and classification tasks [25, 40]. When using the rectified linear unit (ReLU) activation function [16] and fitting the model with stochastic gradient descent (SGD) or BFGS minimization techniques [23, 34, 38], the model built by a multilayer perceptron uses layers  $l : \mathbb{R}^i \rightarrow \mathbb{R}^j$  defined by

$$l(u) = (u^t W_l + c_l)_+,$$

where  $c_l \in \mathbb{R}^j$  and  $W_l$  is the  $i \times j$  weight matrix for layer  $l$ . In this form, the multilayer perceptron (MLP) produces a piecewise linear model of the input data. The computational complexity of training a multilayer perceptron is  $\mathcal{O}(ndm)$ , where  $m$  is determined by the sizes of the layers of the network and the stopping criterion of the minimization used for finding weights. This paper uses an MLP built from Keras and Tensorflow to perform regression [1, 11] with ten hidden layers each having thirty two nodes (a total of approximately ten thousand parameters), ReLU activation, and five thousand epochs of SGD for training.

### 3 Multivariate Interpolation

The following interpolation techniques demonstrate a reasonable variety of approaches to interpolation. All of the presented interpolants produce approximations that are continuous in value, which is often a desirable property in applied approximation problems.

#### 3.1 Delaunay

The Delaunay triangulation is a well-studied geometric technique for producing an interpolant [29]. The Delaunay triangulation of a set of data points into simplices is such that there are no data points inside the sphere defined by the vertices of each simplex. For a  $d$ -simplex  $S$  with vertices  $x^{(0)}, x^{(1)}, \dots, x^{(d)}$ , and function values  $f(x^{(i)})$ ,  $i = 0, \dots, d$ ,  $y \in S$  is a unique convex combination of the vertices,

$$y = \sum_{i=0}^d w_i x^{(i)}, \quad \sum_{i=0}^d w_i = 1, \quad w_i \geq 0, \quad i = 0, \dots, d,$$

and the Delaunay interpolant  $\hat{f}(y)$  at  $y$  is given by

$$\hat{f}(y) = \sum_{i=0}^d w_i f(x^{(i)}).$$

The computational complexity of Delaunay interpolation (for the implementation used [9]) is  $\mathcal{O}(knd^3)$ . Given pathological data the entire triangulation could be computed with  $k = n^{\lceil d/2 \rceil}$ , but the average case yields  $k = d \log d$  and is capable of scaling reasonably to  $d \leq 50$ . In the present application, a Delaunay simplex  $S$  containing  $y$  is found, then the  $d + 1$  vertices (points in  $X$ ) of  $S$  are used to assign weights to each vertex and produce the predicted function value for point  $y$ .

### 3.2 Modified Shepard

The modified Shepard method used here (ShepMod) generates a continuous approximation based on Euclidean distance and resembles a nearest neighbor interpolant [15]. This model is a type of *metric interpolation*, also called a Shepard method [24, 41]. The interpolant has the form

$$p(x) = \frac{\sum_{k=1}^n W_k(x) f(x^{(k)})}{\sum_{k=1}^n W_k(x)},$$

where  $W_k(x) = (r_k - \|x - x^{(k)}\|)_+^2 / \|x - x^{(k)}\|_2^2$  and  $r_k \in \mathbb{R}$  is the smallest radius such that at least  $d+1$  other points  $x^{(j)}$ ,  $j \neq k$ , are inside the closed Euclidean ball of radius  $r_k$  about  $x^{(k)}$ . The computational complexity of ShepMod is  $\mathcal{O}(n^2 d)$ . This paper uses a Fortran 95 implementation of ShepMod derived from SHEPPACK [42].

### 3.3 Linear Shepard

The linear Shepard method (LSHEP) is a blending function using local linear interpolants, a special case of the general Shepard algorithm [42]. The interpolant has the form

$$p(x) = \frac{\sum_{k=1}^n W_k(x) P_k(x)}{\sum_{k=1}^n W_k(x)},$$

where  $W_k(x)$  is a locally supported weighting function and  $P_k(x)$  is a local linear approximation to the data satisfying  $P_k(x^{(k)}) = f(x^{(k)})$ . The computational complexity of LSHEP is  $\mathcal{O}(n^2 d^3)$ . This paper uses the Fortran 95 implementation of LSHEP in SHEPPACK [42].

### 3.4 Box Splines

The box spline model used here is a **sparse grid** interpolation technique built from overlapping box splines [6]. The box splines serve as basis functions that are shifted and scaled to have support over box shaped regions. The boxes are constructed in a way to guarantee a covering of the domain [33]. Given a set of box splines  $\{b^{x^{(i)}}\}$  with the iterative box properties outlined in [33] and anchored at interior points  $\{x^{(i)}\}$ ,

$$\hat{f}(y) = \frac{\sum_{i=1}^n b^{x^{(i)}}(y) f(x^{(i)})}{\sum_{i=1}^n b^{x^{(i)}}(y)}.$$

Note that the box splines always satisfy  $b^{x^{(i)}}(x^{(j)}) = \delta_{ij}$  and  $b^{x^{(i)}}(y) \geq 0$ . The computational complexity of interpolation via the box spline model is  $\mathcal{O}(n^2d)$ .

### 3.5 Voronoi

The nearest neighbor algorithm [15] is a well-studied technique for classification and approximation. Nearest neighbor inherently utilizes the convex region  $C^{x^{(i)}}$  (Voronoi cell [19]) consisting of all points closer to  $x^{(i)}$  than to any other point  $x^{(j)}$ . The Voronoi model smooths the nearest neighbor approximation by utilizing the Voronoi cells to define support via a generic basis function  $v : \mathbb{R}^d \rightarrow \mathbb{R}_+$  given by

$$v^{x^{(i)}}(y) = \left( 1 - \frac{\|y - x^{(i)}\|_2}{2 h(y - x^{(i)} \mid x^{(i)})} \right)_+,$$

where  $h(w \mid x^{(i)})$  is the distance between  $x^{(i)}$  and the boundary of the Voronoi cell  $C^{x^{(i)}}$  in the direction  $w$ .  $v^{x^{(i)}}(x^{(j)}) = \delta_{ij}$  and  $v^{x^{(i)}}$  has local support, giving the interpolated value

$$f(y) = \frac{\sum_{i=1}^n v^{x^{(i)}}(y) f(x^{(i)})}{\sum_{i=1}^n v^{x^{(i)}}(y)},$$

where  $0 \leq v^{x^{(i)}}(y) \leq 1$ . The computational complexity of interpolation via this Voronoi model is  $\mathcal{O}(n^2d)$ . All of the approximations are an interpolant involving a convex combination of known function values  $f(x^{(i)})$ .

## 4 Measuring Error

When the range of an approximation is the real numbers, error is reported with summary statistics including: min absolute error, max absolute error, and absolute error quartiles. When the range of an approximation is the space of cumulative distribution functions, the Kolmogorov-Smirnov statistic (max-norm difference between the functions) is used.

A hurdle when modeling function-valued outputs such as cumulative distribution functions (CDFs) or probability density functions (PDFs) is that certain properties must be maintained. It is necessary that a PDF  $f : \mathbb{R} \rightarrow \mathbb{R}$  have the properties  $f(x) \geq 0$  and  $\int_{-\infty}^{\infty} f(x) dx = 1$ . However, for a CDF  $F : \mathbb{R} \rightarrow \mathbb{R}$  the properties are  $F(x) \in [0, 1]$  and  $F(x)$  is absolutely continuous and nondecreasing. This work utilizes the fact that a convex combination of CDFs (or PDFs) results in a valid CDF (or PDF). Given  $G(x) = \sum_i w_i F_i(x)$ ,  $\sum_i w_i = 1$ ,  $w_i \geq 0$ , and each  $F_i$  is a valid CDF,  $G$  must also be a valid CDF. A demonstration of how this is applied can be seen in Figure 1.

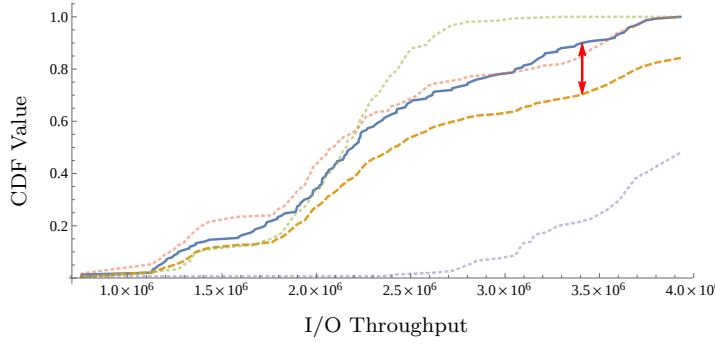


**Fig. 1** In this HPC I/O example, the general methodology for predicting a CDF and evaluating error can be seen. The Delaunay method chose three source distributions (dotted lines) and assigned weights  $\{.3, .4, .3\}$  (top to bottom at arrow). The weighted sum of the three known CDFs produces the predicted CDF (dashed line). The KS Statistic (arrow) computed between the true CDF (solid line) and predicted CDF (dashed line) is 0.2 for this example. For this example the KS test null hypothesis is rejected at  $p$ -value 0.01, however it is not rejected at  $p$ -value 0.001.

The performance of approximation techniques that predict probability functions can be analyzed through a variety of summary statistics. This work uses the max absolute difference, also known as the Kolmogorov-Smirnov (KS) statistic [30] for its compatibility with the KS test.

The two-sample KS test is a useful nonparametric test for comparing two CDFs while only assuming stationarity, finite mean, and finite variance. The null hypothesis (that two CDFs come from the same underlying distribution) is rejected at level  $p \in [0, 1]$  when

$$KS > \sqrt{-\frac{1}{2} \ln\left(\frac{p}{2}\right)} \sqrt{\frac{1}{n_1} + \frac{1}{n_2}},$$

with distribution sample sizes  $n_1, n_2 \in \mathcal{N}$ . For all applications of the KS test presented in this work  $n_1 = n_2$ . An example of the round-trip prediction methodology from known and predicted distributions to the calculation of error can be seen in Figure 1. A brief listing of relevant statistical terms used throughout this work is provided in the Appendix (Section A).

## 5 Theoretical Error Bound

This section presents the theoretical results bounding the error of (piecewise) linear interpolation. The error analysis relies on linear interpolation for three reasons: (1) second order results can be obtained utilizing a Lipschitz constant on the gradient of a function, rather than standard Lipschitz bounds; (2) the results directly apply to Delaunay interpolation; and (3) multiple other interpolants in this paper compute predictions as convex combinations of observed function values, which may allow for straight forward extensions of this error bound.



**Lemma 1** Let  $S \subset \mathbb{R}^d$  be open and convex,  $f : \mathbb{R}^d \rightarrow \mathbb{R}$ , and  $\nabla f \in Lip_{(\gamma, \|\cdot\|_2)}(S)$ , the set of  $\gamma$ -Lipschitz continuous functions in the 2-norm. Then for all  $x, y \in S$

$$|f(y) - f(x) - \langle \nabla f(x), y - x \rangle| \leq \frac{\gamma \|y - x\|_2^2}{2}.$$

*Proof.* Consider the function  $g(t) = f((1-t)x + ty)$ ,  $0 \leq t \leq 1$ , whose derivative  $g'(t) = \langle \nabla f((1-t)x + ty), y - x \rangle$  is the directional derivative of  $f$  in the direction  $(y - x)$ .

$$\begin{aligned} |f(y) - f(x) - \langle \nabla f(x), y - x \rangle| &= |g(1) - g(0) - g'(0)| \\ &= \left| \int_0^1 g'(t) - g'(0) dt \right| \\ &\leq \int_0^1 |g'(t) - g'(0)| dt \\ &= \int_0^1 \left| \langle \nabla f((1-t)x + ty) - \nabla f(x), y - x \rangle \right| dt \\ &\leq \int_0^1 \|\nabla f((1-t)x + ty) - \nabla f(x)\|_2 \|y - x\|_2 dt \\ &\leq \int_0^1 (\gamma \|y - x\|_2) (\|y - x\|_2) t dt \\ &= \frac{\gamma \|y - x\|_2^2}{2}. \end{aligned}$$

□

**Lemma 2** Let  $x, y, v_i \in \mathbb{R}^d$ ,  $c_i \in \mathbb{R}$ , and  $|\langle y - x, v_i \rangle| \leq c_i$  for  $i = 1, \dots, d$ . If  $M = (v_1, \dots, v_d)$  is nonsingular, then

$$\|y - x\|_2^2 \leq \frac{1}{\sigma_d^2} \sum_{i=1}^d c_i^2,$$

where  $\sigma_d$  is the smallest singular value of  $M$ .

*Proof.* Using the facts that  $M$  and  $M^t$  have the same singular values, and  $\|M^t w\|_2 \geq \sigma_d \|w\|_2$ , gives

$$\begin{aligned} \|y - x\|_2^2 &\leq \frac{\|M^t(y - x)\|_2^2}{\sigma_d^2} \\ &= \frac{1}{\sigma_d^2} \sum_{i=1}^d \langle y - x, v_i \rangle^2 \\ &\leq \frac{1}{\sigma_d^2} \sum_{i=1}^d c_i^2. \end{aligned}$$

□

**Lemma 3** Given  $f, \gamma, S$  as in *Lemma 1*, let  $X = \{x_0, x_1, \dots, x_d\} \subset S$  be the vertices of a  $d$ -simplex, and let  $\hat{f}(x) = \langle c, x - x_0 \rangle + f(x_0)$ ,  $c \in \mathbb{R}^d$  be the linear function interpolating  $f$  on  $X$ . Let  $\sigma_d$  be the smallest singular value of the matrix  $M = (x_1 - x_0, \dots, x_d - x_0)$ , and  $k = \max_{1 \leq j \leq d} \|x_j - x_0\|_2$ . Then

$$\|\nabla f(x_0) - c\|_2 \leq \sqrt{d} \frac{\gamma k^2}{2\sigma_d}.$$

*Proof.* Consider  $f(x) - \hat{f}(x)$  along the line segment  $z(t) = (1-t)x_0 + tx_j$ ,  $0 \leq t \leq 1$ . By Rolle's Theorem, for some  $0 < \hat{t} < 1$ ,  $\langle \nabla f(z(\hat{t})) - c, x_j - x_0 \rangle = 0$ . Now

$$\begin{aligned} |\langle \nabla f(x_0) - c, x_j - x_0 \rangle| &= |\langle \nabla f(x_0) - \nabla f(z(\hat{t})) + \nabla f(z(\hat{t})) - c, x_j - x_0 \rangle| \\ &= |\langle \nabla f(x_0) - \nabla f(z(\hat{t})), x_j - x_0 \rangle| \\ &\leq \|\nabla f(x_0) - \nabla f(z(\hat{t}))\|_2 \|x_j - x_0\|_2 \\ &\leq \gamma \|x_0 - z(\hat{t})\|_2 \|x_j - x_0\|_2 \\ &\leq \frac{\gamma}{2} \|x_j - x_0\|_2^2 \leq \frac{\gamma k^2}{2}, \end{aligned}$$

for all  $1 \leq j \leq d$ . Using *Lemma 2*,

$$\|\nabla f(x_i) - c\|_2^2 \leq \frac{d}{\sigma_d^2} (\gamma k^2/2)^2 \implies \|\nabla f(x_i) - c\|_2 \leq \sqrt{d} \frac{\gamma k^2}{2\sigma_d}.$$

□

**Theorem** Under the assumptions of *Lemma 1* and *Lemma 3*, for  $z \in S$ ,

$$|f(z) - \hat{f}(z)| \leq \frac{\gamma \|z - x_0\|_2^2}{2} + \sqrt{d} \frac{\gamma k^2}{2\sigma_d} \|z - x_0\|_2.$$

*Proof.* Let  $v = \nabla f(x_0) - c$ , where  $\|v\|_2 \leq \sqrt{d} \gamma k^2 / (2\sigma_d)$  by *Lemma 3*. Now

$$\begin{aligned} |f(z) - \hat{f}(z)| &= |f(z) - f(x_0) - \langle c, z - x_0 \rangle| \\ &= |f(z) - f(x_0) - \langle \nabla f(x_0) - v, z - x_0 \rangle| \\ &= |f(z) - f(x_0) - \langle \nabla f(x_0), z - x_0 \rangle + \langle v, z - x_0 \rangle| \\ &\leq |f(z) - f(x_0) - \langle \nabla f(x_0), z - x_0 \rangle| + |\langle v, z - x_0 \rangle| \\ &\leq |f(z) - f(x_0) - \langle \nabla f(x_0), z - x_0 \rangle| + \|v\|_2 \|z - x_0\|_2 \\ &\leq |f(z) - f(x_0) - \langle \nabla f(x_0), z - x_0 \rangle| + \sqrt{d} \frac{\gamma k^2}{2\sigma_d} \|z - x_0\|_2 \\ &\leq \frac{\gamma \|z - x_0\|_2^2}{2} + \sqrt{d} \frac{\gamma k^2}{2\sigma_d} \|z - x_0\|_2, \end{aligned}$$

where the last inequality follows from *Lemma 1*.

□

In summary, the approximation error of a linear (simplicial) interpolant tends quadratically towards zero when approaching observed data only when the diameter of the simplex is also reduced at a proportional rate. Only linear convergence to the true function can be achieved in practice, without the incorporation of additional observations. Notice that the approximation error is largely determined by the spacing of observed data. Predictions made by simplices whose vertices are not well-spaced (i.e., have large diameter, or are nearly contained in a hyperplane) have higher error.

The theoretical error bound is tight and that can be observed with the test function  $q(x) = \|x\|_2^2$ ,  $x \in \mathbb{R}^d$  for  $d \in \mathcal{N}$ , and the simplex defined by vertices  $X = \{\mathbf{0}, e_1, \dots, e_d\}$  where  $e_i$  is  $i$ -th unit vector in  $\mathbb{R}^d$  and boldface numbers represent the respective number times the one vector in  $\mathbb{R}^d$ . The relevant constants to the error bound are

$$\gamma = 2, \quad \sigma_d = 1, \quad k = 1, \quad x_0 = \mathbf{0}, \quad \hat{q}(x) = \langle \mathbf{1}, x - \mathbf{0} \rangle + q(\mathbf{0}).$$

Noting that  $q(\mathbf{0}) = 0$ , the approximation error at  $z = -\mathbf{1}/2$  is

$$\begin{aligned} |q(z) - \hat{q}(z)| &= \left| \|z\|_2^2 - \langle \mathbf{1}, z \rangle \right| \\ &= \left| \frac{d}{4} + \frac{d}{2} \right| = \frac{3d}{4}, \end{aligned}$$

while plugging the constants into the error bound from the theorem gives

$$\begin{aligned} |q(z) - \hat{q}(z)| &\leq \frac{\gamma \|z - x_0\|_2^2}{2} + \sqrt{d} \frac{\gamma k^2}{2\sigma_d} \|z - x_0\|_2 \\ &= \|z\|_2^2 + \sqrt{d} \|z\|_2 \\ &= \frac{d}{4} + \frac{d}{2} = \frac{3d}{4}. \end{aligned}$$

Acknowledging that the error bound is tight, it may be of interest to observe the error of piecewise linear approximation techniques on an analytic test function.

### 5.1 Demonstration on an Analytic Test Function

The theoretical results constructed in Section 5 for (piecewise) linear interpolation are promising and apply directly to Delaunay interpolation, however they are difficult to interpret in context with approximation algorithms that do not have similar known uniform error bounds. For that reason, an analytic function is used to measure the error of a piecewise linear interpolant (Delaunay) and a piecewise linear regressor (the MLP) when provided an increasing amount of data with varying levels of random noise.

The test function chosen here for analysis resembles the *oscillatory* function used by [2]. However, a slight modification is made to remove the simple dot

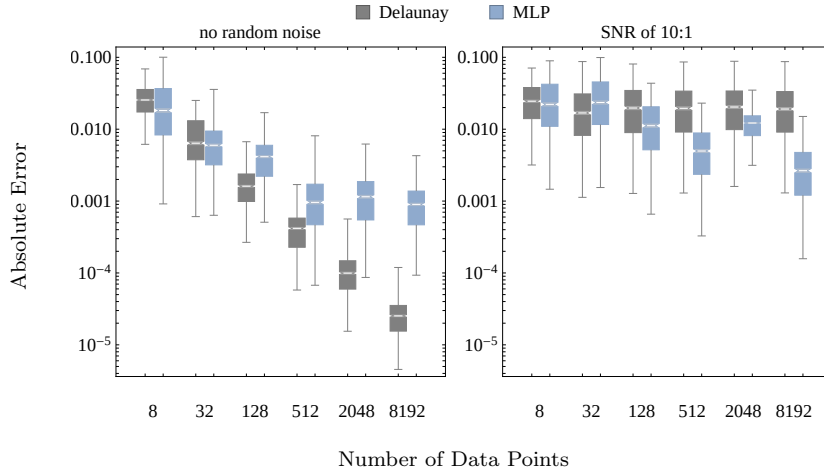


**Fig. 2** Delaunay and MLP approximations are constructed from Fekete points over the unit cube evaluating the test function  $f(x) = \cos(\|x\|_2)$  for  $x \in \mathbb{R}^2$ . These boxes depict the median (middle bar), median 95% confidence interval (cones), quartiles (box edges), and fences at 3/2 interquartile range (whiskers) of absolute prediction error for each model at 1000 random evaluation points. The left plot observes a perfect interpolation problem with exact evaluations of  $f$ . The right plot observes a regression problem with uniform random noise increasing or decreasing evaluations of  $f$  by up to 10%. Both axes are log scaled.

product structure (which is favorable for the MLP). Let  $f(x) = \cos(\|x\|_2)$  for  $x \in \mathbb{R}^d$  where  $d$  is either 2 (Fig. 2) or 20 (Fig. 3). This function has a bounded change in gradient magnitude with respect to the 2-norm and hence meets the necessary Lipschitz condition for the error bound. Data points and approximation points for this test will be within the unit cube  $[0, 1]^d$ .

As seen in the worst-case demonstration after the theorem, the error of a linear interpolant constructed from well spaced points is dominated by the distance to the nearest data point. In order to uniformly decrease to distance to the nearest data point across the unit cube, exponentially more data points must be available for approximation. For this experiment the chosen  $N = 2(4^i)$  for  $i \in (1, \dots, 6)$  points are kept well spaced by computing approximate Fekete points from a tensor-product of Chebyshev nodes. Fekete points have a history in potential theory [27] and they are most generally defined as those points that maximize the (absolute value of) the Vandermonde determinant. Here, the QR method outlined in [7] is used to identify approximate Fekete points from a Vandermonde matrix. A multivariate polynomial basis is constructed consisting of all interactions up to order  $j$  such that  $1 + \sum_{i=1}^j d^i$  is at least  $2N$ . In order to keep the task computationally tractable, a sample of at most  $2N$  nodes and  $2N$  basis functions are used when computing the Vandermonde matrix.

Finally an additional variable is added to this test problem by incorporating random uniform noise into the evaluations of  $f$ . For each test two experiments

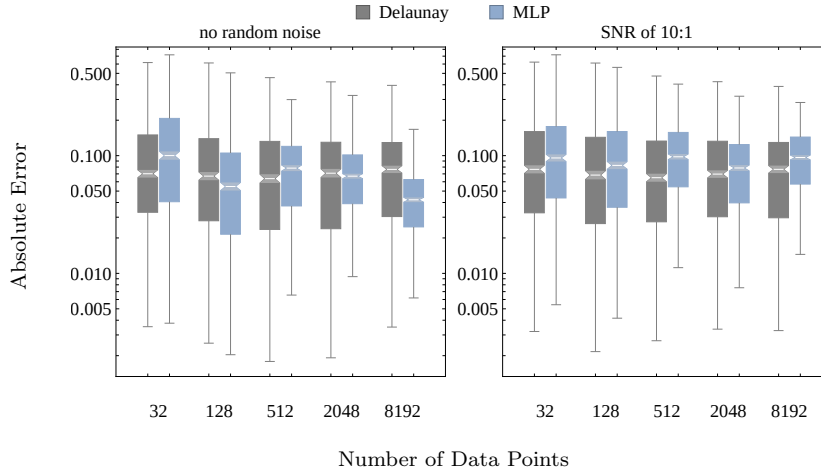


**Fig. 3** Delaunay and MLP approximations are constructed from Fekete points over the unit cube evaluating the test function  $f(x) = \cos(\|x\|_2)$  for  $x \in \mathbb{R}^{20}$ . These boxes depict the median (middle bar), median 95% confidence interval (cones), quartiles (box edges), and fences at  $3/2$  interquartile range (whiskers) of absolute prediction error for each model at 1000 random evaluation points. The left plot observes a perfect interpolation problem with exact evaluations of  $f$ . The right plot observes a regression problem with uniform random noise increasing or decreasing evaluations of  $f$  by up to 10%. Both axes are log scaled.

are executed, one with exact function evaluations (for interpolation) and one with a constant signal-to-noise (SNR) ratio of 10:1 (for regression).

The bound from the theorem suggests that exponentially increasing the number of data points should result in a quadratically decreasing error. The  $d = 2$  test seen on the left half of Figure 2 shows an accelerating decrease in error for Delaunay and also shows the eventual accuracy plateau obtained by a parametric regression form (the MLP, at roughly 500 points). On the right hand side of Figure 2 the random noise clearly prohibits Delaunay from converging on  $f$ , while the MLP is able to improve its approximation with more data points on average. The convergence result for a relatively low-dimension problem like this is expected. However, intuition surrounding convergence fails for higher dimension problems.

In Figure 3 a  $d = 20$  version of the test function presents a significantly more challenging approximation problem than its counterpart in low dimension. The same increase in number of data points from 32 to 8192 causes no apparent improvement in approximation for either the noise-free nor the noisy problems. Perhaps unexpectedly, the interpolation technique performs better than the regression technique on the noisy test (right) in Figure 3, and worse than the regression technique on the noise-free test (left). This result emphasizes the relevance of interpolation for problems in high dimension. It also reveals that the outcome of some regressions can be unfortunately sensitive to random chance (the approximation gets worse when adding more data points in the noise-free case).

In summary, the regime of interpolation is much greater for moderate to high dimension problems, even for functions with random noise incorporated into their evaluation. Acknowledging the viability of interpolation for problems in moderate dimension, the next section will consider real-world problems of similar proportion (thousands of examples in tens of dimensions).

## 6 Data and Empirical Analysis

This section extends the comparison of interpolation and regression algorithms to a sample of real-world problems. Five different data sets of varying dimension and application are utilized to construct approximations and compare the accuracy of different techniques.

In the following five subsections the sources and targets of each test data set are described, as well as challenges and limitations related to approximating these data. The distribution of response values being modeled is presented followed by the distribution of approximation errors for each algorithm. The plots for all five data sets have the same format.

All five data sets are rescaled such that the domain of approximation is the unit hypercube. The range of the first four data sets is the real numbers, while the range of the fifth data set is the space of cumulative distribution functions. All approximation techniques are applied to the first four data sets, while only those interpolants whose approximations are convex combinations of observed data are applied to the final data set.

All approximations are constructed using  $k$ -fold cross validation as described in [26] with  $k = 10$ . This approach randomly partitions data into  $k$  (nearly) equal sized sets. Each algorithm is then evaluated by constructing an approximation over each unique union of  $k - 1$  elements of the partition, making predictions for points in the remaining element. As a result, each observed data point is used in the construction of  $k - 1$  different approximations and is approximated exactly once. The  $k$ -fold cross validation method is data-efficient and provides an unbiased estimate of the expected prediction error [26], however it should be noted that neither this method nor others can provide a universally unbiased estimator for the variance of prediction error [4].

In addition to the figures displaying approximation results for each data set, tables of accompanying numerical results are located in the Appendix (Section A). All of the test data sets capture underlying functions that are almost certainly stochastic. As described in Section 1, regression techniques appear most appropriate for these problems. However, typically data grows exponentially more sparse with increasing dimension. Given sparse data regressors tend towards interpolation and, as demonstrated in Section 5.1, interpolants produce similar (if not identical) results. It is presumed that interpolants are equally viable approximation techniques on these problems.

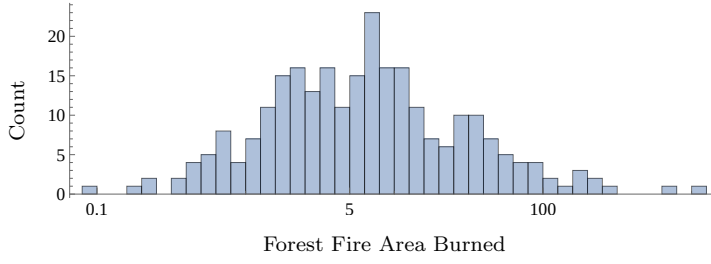


**Fig. 4** Histogram of forest fire area burned under recorded weather conditions. The data is presented on a  $\ln$  scale because most values are small with exponentially fewer fires on record that burn large areas.

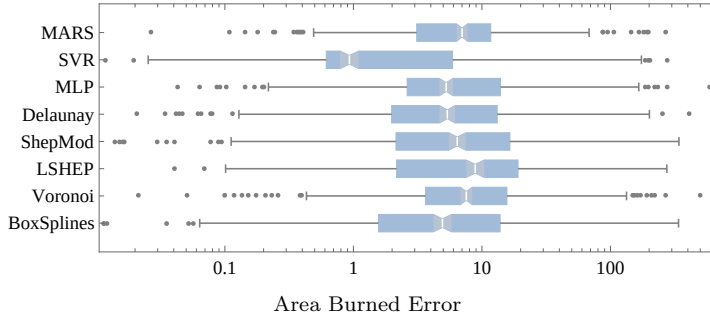


**Fig. 5** All models are applied to approximate the amount of area that would be burned given environment conditions. 10-fold cross validation as described in the beginning of Section 6 is used to evaluate each algorithm. This results in exactly one prediction from each algorithm for each data point. These boxes depict the median (middle bar), median 95% confidence interval (cones), quartiles (box edges), fences at  $3/2$  interquartile range (whiskers), and outliers (dots) of absolute prediction error for each model. Similar to Figure 4, the errors are presented on a  $\ln$  scale. The numerical data corresponding to this figure is provided in Table 3 in the Appendix.

### 6.1 Forest Fire ( $n = 504$ , $d = 12$ )

The forest fire data set [13] describes the area of Montesinho park burned over months of the year along with environmental conditions. The twelve dimensions being used to model burn area are the  $x$  and  $y$  spatial coordinates of burns in the park, month of year (mapped to  $x$ ,  $y$  coordinates on a unit circle), the FPMC, DMC, DC, and ISI indices (see source for details), the temperature, relative humidity, wind speed, and outdoor rain. The original analysis of this data set demonstrated it to be difficult to model, likely due to the skew in response values.

As suggested by Figure 5, the SVR has the lowest absolute prediction errors for 80% of the data, with MLP and Delaunay being the nearest overall competitors. The effectiveness of SVR on this data suggests the underlying function can be defined by relatively few parameters, as well as the importance of capturing the low-burn-area data points.

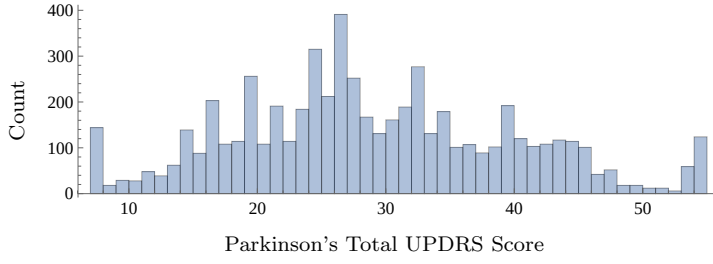


**Fig. 6** Histogram of the Parkinson's patient total UPDRS clinical scores that will be approximated by each algorithm.

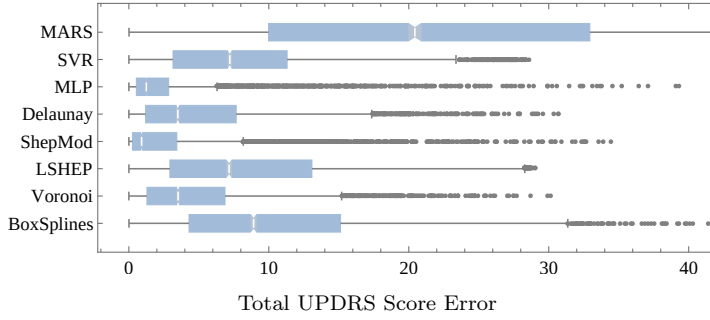


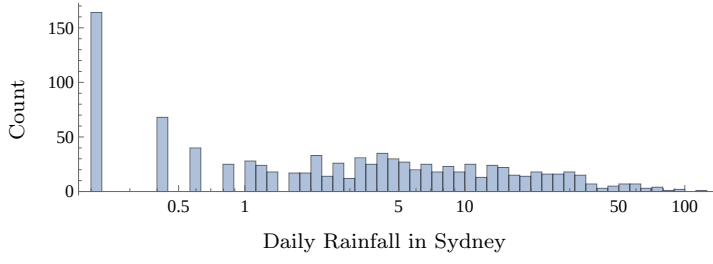
**Fig. 7** All models are applied to approximate the total UPDRS score given audio features from patients' home life, using 10-fold cross validation. These boxes depict the median (middle bar), median 95% confidence interval (cones), quartiles (box edges), fences at 3/2 interquartile range (whiskers), and outliers (dots) of absolute prediction error for each model. The numerical data corresponding to this figure is provided in Table 5 in the Appendix.

## 6.2 Parkinson's Telemonitoring ( $n = 5875$ , $d = 19$ )

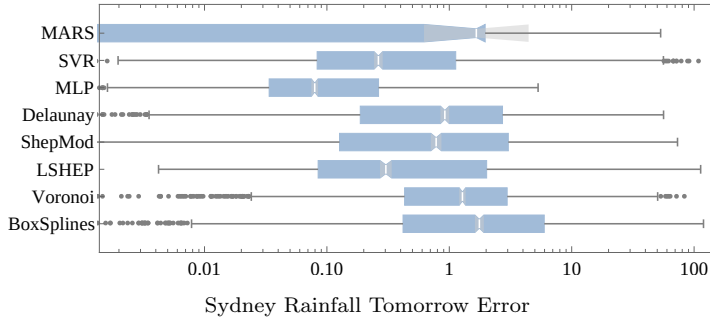
The second data set for evaluation [43] is derived from a speech monitoring study with the intent to automatically estimate Parkinson's disease symptom development in Parkinson's patients. The function to be approximated is a time-consuming clinical evaluation measure referred to as the UPDRS score. The total UPDRS score given by a clinical evaluation is estimated through 19 real numbers generated from biomedical voice measures of in-home sound recordings.

Figure 7 shows the ShepMod algorithm has the lowest minimum, first quartile, and median of absolute errors for this problem, while providing the best prediction 66% of the time. The MLP has the lowest third quartile and provides the best prediction for 32% of approximations. The dominance of ShepMod may be due in part to regular-interval total UPDRS scores provided by clinicians, favoring a nearest-neighbor strategy of prediction.





**Fig. 8** Histogram of daily rainfall in Sydney, Australia, presented on a  $\ln$  scale because the frequency of larger amounts of rainfall is significantly less. There is a peak in occurrence of the value 0, which has a notable effect on the resulting model performance.



**Fig. 9** All models are applied to approximate the amount of rainfall expected on the next calendar day given various sources of local meteorological data, using 10-fold cross validation. These boxes depict the median (middle bar), median 95% confidence interval (cones), quartiles (box edges), fences at 3/2 interquartile range (whiskers), and outliers (dots) of absolute prediction error for each model. The errors are presented on a  $\ln$  scale, mimicking the presentation in Figure 8. The numerical data corresponding to this figure is provided in Table 7 in the Appendix.

### 6.3 Australian Daily Rainfall Volume ( $n = 2609$ , $d = 23$ )

The third data set for the total daily rainfall in Sydney, Australia [45] provides a slightly higher dimensional challenge for the interpolants and regressors. This data is composed of many meteorological readings from the region in a day including: min and max temperatures, sunshine, wind speed directions (converted to coordinates on a circle), wind speeds, and humidities throughout the day, day of the year (converted to coordinates on a circle), and the model must predict the amount of rainfall tomorrow.

While Figure 8 makes MARS look far better than other techniques, it only provides the best prediction for 11% of points. The MLP has the lowest absolute error for 56% of points and LSHEP is best for 28%. MARS likely achieves such a low first quartile due to the high occurrence of the value zero in the data.

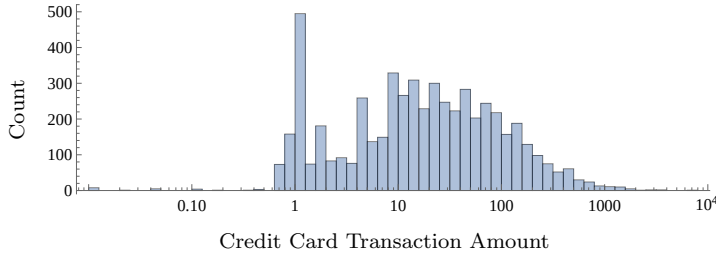


**Fig. 10** Histogram of credit card transaction amounts, presented on a  $\ln$  scale. The data contains a notable frequency peak around \$1 transactions. Fewer large purchases are made, but some large purchases are in excess of five orders of magnitude greater than the smallest purchases.

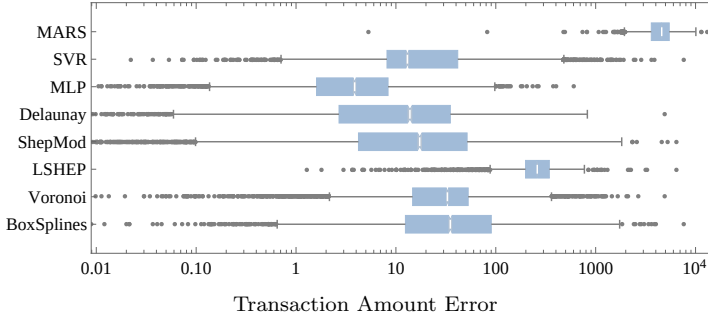


**Fig. 11** All models are applied to approximate the expected transaction amount given transformed (and obfuscated) vendor and customer-descriptive features, using 10-fold cross validation. These boxes depict the median (middle bar), median 95% confidence interval (cones), quartiles (box edges), fences at  $3/2$  interquartile range (whiskers), and outliers (dots) of absolute prediction error for each model. The absolute errors in transaction amount predictions are presented on a  $\ln$  scale, just as in Figure 10. The numerical data corresponding to this figure is provided in Table 9 in the Appendix.

#### 6.4 Credit Card Transaction Amount ( $n = 5562$ , $d = 28$ )

The fourth test data set, and the final with a real-valued range, is a collection of credit card transactions [37]. The provided data carries no direct real-world meaning, being the output of a principle component analysis on the original hidden source data. This obfuscation is done to protect the information of the credit card users. This data has the largest dimension of all considered, at 28. A model for this data predicts the transaction amount given the vector of principle component information.

As can be seen in Figure 11, the MLP outperforms all other algorithms at the first, second, third, and fourth quartiles. The MLP produces the lowest absolute error prediction for 80% of transactions, Delaunay bests the remaining 20%. It is likely that with less data, Delaunay would be the best performer.

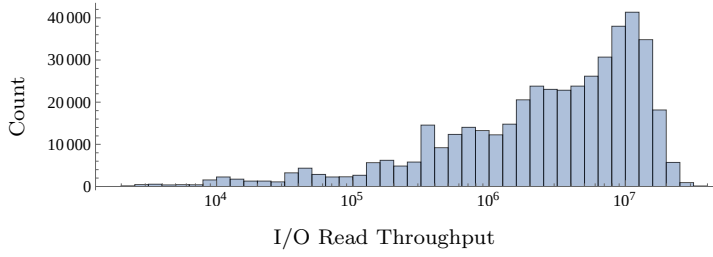


**Fig. 12** Histogram of the raw throughput values recorded during all IOzone tests across all system configurations. The distribution is skewed right, with few tests having significantly higher throughput than most others. The data is presented on a ln scale.

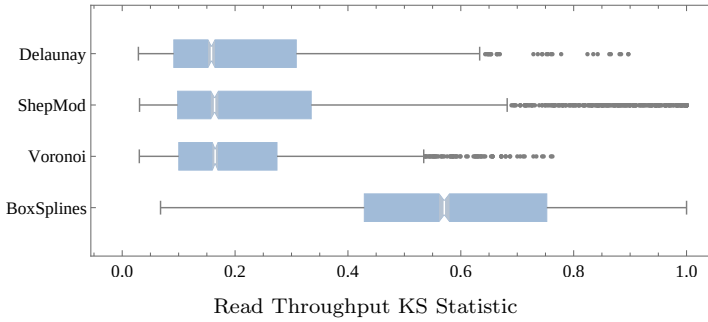


**Fig. 13** The models directly capable of predicting distributions are applied to predicting the expected CDF of I/O throughput at a previously unseen system configuration, using 10-fold cross validation. The KS statistic (max norm) between the observed distribution at each system configuration and the predicted distribution is recorded and presented above. Note that the above figure is *not* log-scaled like Figure 12. The numerical data corresponding to this figure is provided in Table 11 in the Appendix.

### 6.5 High Performance Computing I/O ( $n = 3016$ , $d = 4$ )

The final of five data sets is derived from [8], which provides four-dimensional distribution data by executing the IOzone benchmark [35] on a computer system and varying the system’s file size, record size, thread count, and CPU frequency. At each configuration, IOzone samples the I/O file-read throughput (in bytes per second) 150 times. Empirical distribution function points are computed from each set of 150 executions, which are interpolated with a piecewise cubic Hermite interpolating polynomial [22] to approximate the CDF. All interpolation algorithms with the exception of LSHEP are used to approximate these CDFs from system configurations.

Delaunay achieves the lowest KS statistic (max norm difference) for 62% of approximations, while Voronoi is best for the remaining 38%. Figure 13 shows that while Delaunay may have more best predictions, the behavior of Voronoi may be preferable.

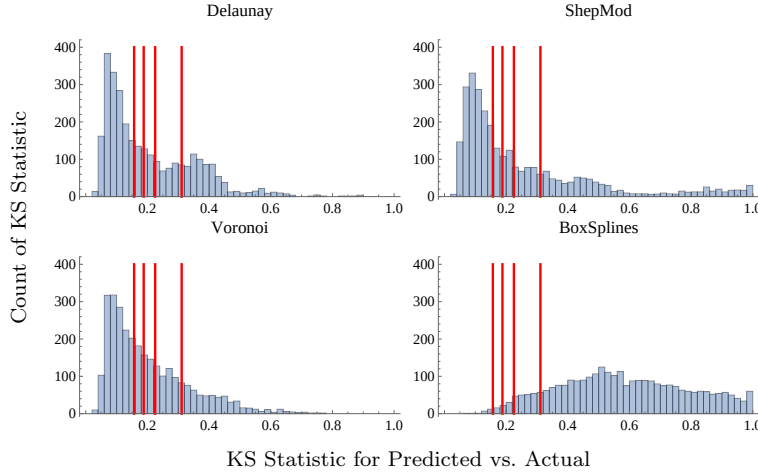


**Fig. 14** Histograms of the prediction error for each interpolant that produces predictions as convex combinations of observed data, using 10-fold cross validation. The histograms show the KS statistics for the predicted throughput distribution versus the actual throughput distribution. The four vertical lines represent cutoff KS statistics given 150 samples for commonly used  $p$ -values 0.05, 0.01, 0.001,  $10^{-6}$ , respectively. All predictions to the right of a vertical line represent CDF predictions that are significantly different (by respective  $p$ -value) from the actual distribution according to the KS test. The numerical counterpart to this figure is presented in Table 1.

	$p = .05$	$p = .01$	$p = .001$	$p = 10^{-6}$
Delaunay	<b>50.3%</b>	43.5%	36.2%	24.7%
ShepMod	51.4%	44.8%	38.1%	27.7%
Voronoi	52.6%	<b>43.4%</b>	<b>34.4%</b>	<b>19.1%</b>
BoxSplines	99.4%	98.5%	96.6%	89.3%

**Table 1** Numerical counterpart of the histogram data presented in Figure 14. The columns display the percent of null hypothesis rejections by the KS-test when provided different selections of  $p$ -values for each algorithm. The algorithm with the lowest rejection rate at each  $p$  is boldface, while the second lowest is italicized.

Figure 14 expands on the KS statistic results presented in Figure 13. Agglomerate errors for each algorithm resemble a Gamma distribution. The percentages of significant prediction errors with varying  $p$ -values are on display in Table 1. When considering the  $p = 0.001$  results for each technique, a little over one third of the predicted CDFs are significantly different from the measured (and presumed) correct CDFs. However, it should be noted that with 150 samples, the error of an empirical distribution function (EDF) can reasonably be upwards of .1, which serves as a rough estimate for the lower limit of achievable error. Globally, only a third of Voronoi predictions fail to capture *all* of the characteristics of the CDFs at new system configurations.

Algorithm	Avg. % Best	Avg. Fit or Prep. Time (s)	Avg. App. Time (s)
MARS	4.5	20.0s	0.001s
SVR	19.5	<b>0.5s</b>	<b>0.0001s</b>
MLP	<b>43.1</b>	200.0s	0.001s
Delaunay	5.2	1.0s	1.0s
ShepMod	18.0	0.7s	<b>0.0001s</b>
LSHEP	8.4	2.0s	<b>0.0001s</b>
Voronoi	0.5	1.0s	0.04s
BoxSplines	3.5	0.8s	0.0005s

**Table 2** This average of Appendix Tables 4, 6, 8, and 10 provides a gross summary of overall results. The columns display (weighted equally by data set, *not* points) the average frequency with which any algorithm provided the lowest absolute error approximation, the average time to fit/prepare, and the average time required to approximate one point. The times have been rounded to one significant digit, as reasonably large fluctuations may be observed due to implementation hardware. Interpolants provide the lowest error approximation for nearly one third of all data, while regressors occupy the other two thirds. This result is obtained without any customized tuning or preprocessing to maximize the performance of any given algorithm. In practice, tuning and preprocessing may have large effects on approximation performance.

## 7 Discussion

Table 2 summarizes results across the four test data sets with real-valued ranges. The interpolants discussed in this paper produce the *best* approximations roughly one third of the time, and produce competitive approximations for almost all data sets. These test problems are almost certainly *stochastic* in nature, but the high dimension leads to greater data sparsity and model construction cost, making interpolation more competitive.

The major advantages to interpolation lie in the near absence of *fit* time. Delaunay, LSHEP, and ShepMod all require pairwise distance calculations, for numerical robustness (Delaunay) and to determine the radii of influence for data points (LSHEP and ShepMod). At least hundreds, and sometimes hundreds of thousands of predictions can be made by the interpolants before the most widely used regressor (MLP) finishes fitting these relatively small data sets. However, the computational complexities of all interpolants presented are greater than linear in either dimension or number of points, whereas the regressors’ nonlinear complexity in dimension generally comes from the model fitting optimization.

The new theoretical results presented in Section 5 directly apply to Delaunay interpolation, however the performance of Delaunay does not appear significantly better than other algorithms on these data sets. This observation may be due to the stochastic nature of the data, but it also speaks to the power of the approximations generated by the different interpolation methods. The strong performance of other interpolants suggests that theoretical results similar to those presented in this work can be achieved for the other interpolants under reasonable assumptions.

Finally, most of the interpolants presented in this work benefit from the ability to model *any* function over real  $d$ -tuples with a range that is closed under convex combinations. In general, error can be quantified by any measure (particularly of interest may be  $L^2$ ,  $L^\infty$ , etc.). The results of the distribution prediction case study indicate that interpolants can effectively predict CDFs. The error analysis for that work relies on the KS statistic, which captures the worst part of any prediction and hence provides a conservatively large estimate of approximation error. The average absolute errors in the predicted CDFs are always lower than the KS statistics. However, the KS statistic was chosen as a metric because of the important surrounding statistical theory. A nonnegligible volume of predictions provide impressively low levels of average absolute error in that final case study.

## 8 Conclusion

The major contributions of this work are: 1) new uniform theoretical error bounds for piecewise linear interpolation in arbitrary dimension (Section 5); 2) an empirical evaluation across real-world problems that demonstrates interpolants produce competitively accurate models of multivariate phenomenon when compared with common regressors for sparse, moderately high dimensional problems (Section 6); and 3) a demonstration that some interpolants generalize to interpolation in function spaces (Section 4), preserving monotonicity (with CDFs, e.g.), neither of which common regressors can do.

The various interpolants discussed in this paper have been demonstrated to effectively approximate multivariate phenomena up to 30 dimensions. The underlying constructions are theoretically straightforward, interpretable, and yield reasonably accurate predictions. Most of the interpolants' computational complexities make them particularly suitable for applications in even higher dimension. The major benefits of interpolation are seen when only a small number of approximations ( $\leq 1000$ ) are made from data and when there are relatively few data points for the dimension (for empirical results presented,  $\log_d n \leq 5$ ). These findings encourage broader application of interpolants to multivariate approximation in science.

## References

1. Abadi, M., Agarwal, A., Barham, P., Brevdo, E., Chen, Z., Citro, C., Corrado, G.S., Davis, A., Dean, J., Devin, M., Ghemawat, S., Goodfellow, I., Harp, A., Irving, G., Isard, M., Jia, Y., Jozefowicz, R., Kaiser, L., Kudlur, M., Levenberg, J., Mané, D., Monga, R., Moore, S., Murray, D., Olah, C., Schuster, M., Shlens, J., Steiner, B., Sutskever, I., Talwar, K., Tucker, P., Vanhoucke, V., Vasudevan, V., Viégas, F., Vinyals, O., Warden, P., Wattenberg, M., Wicke, M., Yu, Y., Zheng, X.: TensorFlow: Large-scale machine learning on heterogeneous systems (2015). URL <https://www.tensorflow.org/>. Software available from tensorflow.org
2. Barthelmann, V., Novak, E., Ritter, K.: High dimensional polynomial interpolation on sparse grids. *Advances in Computational Mathematics* **12**(4), 273–288 (2000)

3. Basak, D., Pal, S., Patranabis, D.C.: Support vector regression. *Neural Information Processing-Letters and Reviews* **11**(10), 203–224 (2007)
4. Bengio, Y., Grandvalet, Y.: No unbiased estimator of the variance of k-fold cross-validation. *Journal of machine learning research* **5**(Sep), 1089–1105 (2004)
5. de Boor, C.: *A Practical Guide to Splines*, vol. 27. Springer-Verlag New York (1978)
6. de Boor, C., Höllig, K., Riemenschneider, S.: *Box Splines*, vol. 98. Springer Science & Business Media (2013)
7. Bos, L., De Marchi, S., Sommariva, A., Vianello, M.: Computing multivariate feke points by numerical linear algebra. *SIAM Journal on Numerical Analysis* **48**(5), 1984–1999 (2010)
8. Cameron, K.W., Anwar, A., Cheng, Y., Xu, L., Li, B., Ananth, U., Bernard, J., Jearls, C., Lux, T.C.H., Hong, Y., Watson, L.T., Butt, A.R.: Moana: Modeling and analyzing i/o variability in parallel system experimental design. *IEEE Transactions on Parallel and Distributed Systems* (2019). DOI 10.1109/TPDS.2019.2892129
9. Chang, T.H., Watson, L.T., Lux, T.C.H., Li, B., Xu, L., Butt, A.R., Cameron, K.W., Hong, Y.: A polynomial time algorithm for multivariate interpolation in arbitrary dimension via the delaunay triangulation. In: *Proceedings of the ACMSE 2018 Conference, ACMSE '18*, pp. 12:1–12:8. ACM, New York, NY, USA (2018). DOI 10.1145/3190645.3190680. URL <http://doi.acm.org/10.1145/3190645.3190680>
10. Cheney, E.W., Light, W.A.: *A Course in Approximation Theory*, vol. 101. American Mathematical Soc. (2009)
11. Chollet, F., et al.: Keras. <https://keras.io> (2015)
12. Clevert, D.A., Unterthiner, T., Hochreiter, S.: Fast and accurate deep network learning by exponential linear units (elus). *arXiv preprint arXiv:1511.07289* (2015)
13. Cortez, P., Morais, A.d.J.R.: A data mining approach to predict forest fires using meteorological data. *13th Portuguese Conference on Artificial Intelligence* (2007)
14. Cortez, P., Silva, A.M.G.: Using data mining to predict secondary school student performance. *Proceedings of 5th Annual Future Business Technology Conference, Porto* (2008)
15. Cover, T., Hart, P.: Nearest neighbor pattern classification. *IEEE Transactions on Information Theory* **13**(1), 21–27 (1967)
16. Dahl, G.E., Sainath, T.N., Hinton, G.E.: Improving deep neural networks for lvcsr using rectified linear units and dropout. In: *IEEE International Conference on Acoustics, Speech and Signal Processing (ICASSP)*, 2013, pp. 8609–8613. IEEE (2013)
17. De Vito, S., Massera, E., Piga, M., Martinotto, L., Di Francia, G.: On field calibration of an electronic nose for benzene estimation in an urban pollution monitoring scenario. *Sensors and Actuators B: Chemical* **129**(2), 750–757 (2008)
18. Dennis Jr, J.E., Schnabel, R.B.: *Numerical Methods for Unconstrained Optimization and Nonlinear Equations*, vol. 16. Siam (1996)
19. Dirichlet, G.L.: Über die reduction der positiven quadratischen formen mit drei unbestimmten ganzen zahlen. *Journal für die Reine und Angewandte Mathematik* **40**, 209–227 (1850)
20. Friedman, J.H.: Multivariate adaptive regression splines. *The Annals of Statistics* pp. 1–67 (1991)
21. Friedman, J.H., the Computational Statistics Laboratory of Stanford University: *Fast mars*. (1993)
22. Fritsch, F.N., Carlson, R.E.: Monotone piecewise cubic interpolation. *SIAM Journal on Numerical Analysis* **17**(2), 238–246 (1980)
23. Goh, G.: Why momentum really works. *Distill* (2017). DOI 10.23915/distill.00006. URL <http://distill.pub/2017/momentum>
24. Gordon, W.J., Wixom, J.A.: Shepards method of metric interpolation to bivariate and multivariate interpolation. *Mathematics of Computation* **32**(141), 253–264 (1978)
25. Hornik, K., Stinchcombe, M., White, H.: Multilayer feedforward networks are universal approximators. *Neural networks* **2**(5), 359–366 (1989)
26. Kohavi, R., et al.: A study of cross-validation and bootstrap for accuracy estimation and model selection. In: *IJCAI*, vol. 14, pp. 1137–1145. Montreal, Canada (1995)
27. Kvær, T., Pommerenke, C.: On the distribution of feketepoints. *Mathematika* **15**(1), 7075 (1968). DOI 10.1112/S0025579300002400

28. Lazos, D., Sproul, A.B., Kay, M.: Optimisation of energy management in commercial buildings with weather forecasting inputs: A review. *Renewable and Sustainable Energy Reviews* **39**, 587–603 (2014)
29. Lee, D.T., Schachter, B.J.: Two algorithms for constructing a delaunay triangulation. *International Journal of Computer & Information Sciences* **9**(3), 219–242 (1980)
30. Lilliefors, H.W.: On the kolmogorov-smirnov test for normality with mean and variance unknown. *Journal of the American Statistical Association* **62**(318), 399–402 (1967)
31. Lux, T.C.H., Pittman, R., Shende, M., Shende, A.: Applications of supervised learning techniques on undergraduate admissions data. In: *Proceedings of the ACM International Conference on Computing Frontiers*, pp. 412–417. ACM (2016)
32. Lux, T.C.H., Watson, L.T., Chang, T.H., Bernard, J., Li, B., Yu, X., Xu, L., Back, G., Butt, A.R., Cameron, K.W., et al.: Nonparametric distribution models for predicting and managing computational performance variability. In: *SoutheastCon 2018*, pp. 1–7. IEEE (2018)
33. Lux, T.C.H., Watson, L.T., Chang, T.H., Bernard, J., Li, B., Yu, X., Xu, L., Back, G., Butt, A.R., Cameron, K.W., et al.: Novel meshes for multivariate interpolation and approximation. In: *Proceedings of the ACMSE 2018 Conference*, p. 13. ACM (2018)
34. Møller, M.F.: A scaled conjugate gradient algorithm for fast supervised learning. *Neural networks* **6**(4), 525–533 (1993)
35. Norcott, W.D.: Iozone filesystem benchmark (2017). URL <http://www.iozone.org>. [Online; accessed 2017-11-12]
36. Pedregosa, F., Varoquaux, G., Gramfort, A., Michel, V., Thirion, B., Grisel, O., Blondel, M., Prettenhofer, P., Weiss, R., Dubourg, V., Vanderplas, J., Passos, A., Cournapeau, D., Brucher, M., Perrot, M., Duchesnay, E.: Scikit-learn: Machine learning in Python. *Journal of Machine Learning Research* **12**, 2825–2830 (2011)
37. Pozzolo, A.D., Caelen, O., Johnson, R.A., Bontempi, G.: Calibrating probability with undersampling for unbalanced classification. In: *IEEE Symposium Series on Computational Intelligence*, pp. 159–166. IEEE (2015). DOI 10.1109/SSCI.2015.33. URL <https://www.kaggle.com/mlg-ulb/creditcardfraud>. [Online; accessed 2019-01-25]
38. Robbins, H., Monro, S.: A stochastic approximation method. *The Annals of Mathematical Statistics* pp. 400–407 (1951)
39. Rudy, J., Cherti, M.: Py-earth: A python implementation of multivariate adaptive regression splines (2017). URL <https://github.com/scikit-learn-contrib/py-earth>. [Online; accessed 2017-07-09]
40. Rumelhart, D.E., Hinton, G.E., Williams, R.J., et al.: Learning representations by back-propagating errors. *Cognitive modeling* **5**(3), 1 (1988)
41. Shepard, D.: A two-dimensional interpolation function for irregularly-spaced data. In: *Proceedings of the 1968 23rd ACM national conference*, pp. 517–524. ACM (1968)
42. Thacker, W.I., Zhang, J., Watson, L.T., Birch, J.B., Iyer, M.A., Berry, M.W.: Algorithm 905: Sheppack: Modified shepard algorithm for interpolation of scattered multivariate data. *ACM Transactions on Mathematical Software (TOMS)* **37**(3), 34 (2010)
43. Tsanas, A., Little, M.A., McSharry, P.E., Ramig, L.O.: Accurate telemonitoring of parkinson's disease progression by noninvasive speech tests. *IEEE Transactions on Biomedical Engineering* **57**(4), 884–893 (2010)
44. Unther Greiner, G., Hormann, K.: Interpolating and approximating scattered 3d-data with hierarchical tensor product b-splines. In: *Proceedings of Chamonix*, p. 1 (1996)
45. Williams, G.J.: Weather dataset rattle package. In: *Rattle: A Data Mining GUI for R*, vol. 1, pp. 45–55. The R Journal (2009). URL <https://www.kaggle.com/jsphyg/weather-dataset-rattle-package>. [Online; accessed 2019-01-25]



## A Appendix

**Statistical Terminology.** A random variable  $X$  is precisely defined by its *cumulative distribution function* (CDF)  $F_X$  and the derivative of the CDF, the *probability density function* (PDF)  $f_X$ . For any possible value of  $X$ , the *percentile* of that value  $x$  is  $100 F(x)$ , the percentage values drawn from  $X$  that would be less than  $x$  as the number of samples tends towards infinity. The *quartiles* of  $X$  are its 25-th, 50-th (median), and 75-th percentiles. The absolute difference between the median and a quartile is an *interquartile range*. Given an independent and identically distributed sample from  $X$  and presuming that  $X$  has finite mean and variance, a *confidence interval* can be drawn about any percentile estimated from the sample. A *confidence interval* describes the probability that a value lies within an interval. The *null hypothesis* is a statement (derived from some test statistic) that can be disqualified with sufficient evidence, and the  $p$  value is the probability of observing a given statistic if the *null hypothesis* is true.

**Raw Numerical Results.** The tables that follow show the precise experimental results for all data sets presented in Section 6. The tests were all run serially on an otherwise idle machine with a CentOS 6.10 operating system and an Intel i7-3770 CPU operating at 3.4 GHz. The detailed performance results in the tables that follow are very much dependent on the problem and the algorithm implementation (e.g., some codes are TOMS software, some industry distributions, and others are from conference paper venues). Different type-face is used to show best performers, however not much significance should be attached to ranking algorithms based on small time (millisecond) differences. The results serve as a demonstration of conceptual validity.

Algorithm	Min	25 <sup>th</sup>	50 <sup>th</sup>	75 <sup>th</sup>	Max
MARS	0.00984	3.11	7.01	<i>11.7</i>	1090.0
SVR	0.0118	<b>0.615</b>	<b>0.931</b>	<b>5.89</b>	1090.0
MLP	0.0426	2.63	5.27	14.0	1090.0
Delaunay	<b>0.0</b>	1.98	5.37	13.1	<i>1080.0</i>
ShepMod	<b>0.0</b>	1.93	6.27	16.0	1090.0
LSHEP	0.04	2.17	8.87	19.1	<b>1070.0</b>
Voronoi	<i>0.00982</i>	3.65	7.56	15.6	1090.0
BoxSpline	<b>0.0</b>	<i>1.27</i>	<i>4.61</i>	12.6	1090.0

**Table 3** This numerical data accompanies the visual provided in Figure 5. The columns of absolute error percentiles correspond to the minimum, first quartile, median, third quartile, and maximum absolute errors respectively. The minimum of each column is boldface, while the second lowest value is italicized. All values are rounded to three significant digits.

Algorithm	% Best	Fit/Prep. Time (s)	App. Time (s)	Total App. Time (s)
MARS	7.3	29.1	0.00137	0.0686
SVR	<b>78.0</b>	<b>0.00584</b>	<i>0.0000620</i>	<i>0.00310</i>
MLP	0.0	32.8	0.000871	0.0436
Delaunay	0.2	0.0151	0.0234	1.18
ShepMod	2.0	<i>0.00634</i>	0.0000644	0.00322
LSHEP	5.1	0.0275	<b>0.0000463</b>	<b>0.00231</b>
Voronoi	0.0	0.0152	0.000396	0.0198
BoxSpline	<i>9.7</i>	0.00724	0.0000978	0.00489

**Table 4** The left above shows how often each algorithm had the lowest absolute error approximating forest fire data in Table 3. On the right columns are median fit time of 454 points, median time for one approximation, and median time approximating 50 points.

Algorithm	Min	25 <sup>th</sup>	50 <sup>th</sup>	75 <sup>th</sup>	Max
MARS	0.00948	9.98	20.4	32.9	863.0
SVR	0.00233	3.15	7.21	11.3	<b>28.6</b>
MLP	0.0000239	<i>0.533</i>	<i>1.25</i>	<b>2.84</b>	39.3
Delaunay	<i>3.72 × 10<sup>-12</sup></i>	1.2	3.5	7.67	30.7
ShepMod	<b>0.0</b>	<b>0.255</b>	<b>0.908</b>	<i>3.43</i>	34.5
LSHEP	0.00254	2.93	7.16	13.1	<i>29.0</i>
Voronoi	<b>0.0</b>	1.29	3.52	6.87	30.1
BoxSpline	0.006	4.3	8.91	15.1	45.3

**Table 5** This numerical data accompanies the visual provided in Figure 7. The columns of absolute error percentiles correspond to the minimum, first quartile, median, third quartile, and maximum absolute errors respectively. The minimum of each column is boldface, while the second lowest value is italicized. All values are rounded to three significant digits.

Algorithm	% Best	Fit/Prep. Time (s)	App. Time (s)	Total App. Time (s)
MARS	0.0	37.9	0.00253	1.48
SVR	0.1	<b>0.859</b>	<i>0.000181</i>	<i>0.106</i>
MLP	<i>32.0</i>	348.0	0.00111	0.653
Delaunay	0.0	2.47	1.22	720.0
ShepMod	<b>66.4</b>	<i>1.13</i>	0.000182	0.107
LSHEP	0.0	2.39	<b>0.000144</b>	<b>0.0845</b>
Voronoi	1.6	2.77	0.0274	16.1
BoxSpline	0.0	1.26	0.000643	0.377

**Table 6** The left above shows how often each algorithm had the lowest absolute error approximating Parkinson’s data in Table 5. On the right columns are median fit time of 5288 points, median time for one approximation, and median time approximating 587 points.

Algorithm	Min	25 <sup>th</sup>	50 <sup>th</sup>	75 <sup>th</sup>	Max
MARS	<i>6.45 × 10<sup>-15</sup></i>	<b>2.70 × 10<sup>-14</sup></b>	1.66	1.96	<i>53.3</i>
SVR	0.0000915	0.0833	0.263	<i>1.13</i>	109.0
MLP	0.0000689	0.0337	<b>0.0795</b>	<b>0.264</b>	<b>5.31</b>
Delaunay	<b>0.0</b>	0.187	0.919	2.72	56.3
ShepMod	<b>0.0</b>	0.0957	0.685	2.9	73.2
LSHEP	<b>0.0</b>	<i>0.0153</i>	<i>0.106</i>	1.17	113.0
Voronoi	<b>0.0</b>	0.43	1.28	2.94	83.8
BoxSpline	<b>0.0</b>	0.342	1.59	5.53	119.0

**Table 7** This numerical data accompanies the visual provided in Figure 9. The columns of absolute error percentiles correspond to the minimum, first quartile, median, third quartile, and maximum absolute errors respectively. The minimum value of each column is boldface, while the second lowest is italicized. All values are rounded to three significant digits.

Algorithm	% Best	Fit/Prep. Time (s)	App. Time (s)	Total App. Time (s)
MARS	10.7	<i>0.151</i>	0.000117	0.0304
SVR	0.0	<b>0.133</b>	<b>0.0000947</b>	<b>0.0246</b>
MLP	<b>60.9</b>	169.0	0.00137	0.356
Delaunay	0.1	0.664	0.886	230.0
ShepMod	3.5	0.265	0.000128	0.0333
LSHEP	<i>28.4</i>	0.874	<i>0.0000975</i>	<i>0.0254</i>
Voronoi	0.2	0.675	0.0270	7.01
BoxSpline	4.1	0.330	0.000406	0.106

**Table 8** Left table shows how often each algorithm had the lowest absolute error approximating Sydney rainfall data in Table 7. On the right columns are median fit time of 2349 points, median time for one approximation, and median time approximating 260 points.

Algorithm	Min	25 <sup>th</sup>	50 <sup>th</sup>	75 <sup>th</sup>	Max
MARS	5.36	3610.0	4580.0	5450.0	13400.0
SVR	0.00706	8.14	<i>13.0</i>	41.6	7690.0
MLP	0.00151	<b>1.6</b>	<b>3.86</b>	<b>8.34</b>	<b>604.0</b>
Delaunay	<b>0.0</b>	<i>2.69</i>	13.8	<i>35.0</i>	<i>4840.0</i>
ShepMod	<b>0.0</b>	4.21	17.3	51.6	6510.0
LSHEP	1.27	199.0	260.0	343.0	6530.0
Voronoi	<i>2.89 × 10<sup>-10</sup></i>	14.7	32.8	52.9	4860.0
BoxSpline	<b>0.0</b>	12.4	35.0	90.1	7690.0

**Table 9** This numerical data accompanies the visual provided in Figure 11. The columns of absolute error percentiles correspond to the minimum, first quartile, median, third quartile, and maximum absolute errors respectively. The minimum value of each column is boldface, while the second lowest is italicized. All values are rounded to three significant digits.

Algorithm	% Best	Fit/Prep. Time (s)	App. Time (s)	Total App. Time (s)
MARS	0.0	22.0	0.00148	0.820
SVR	0.0	<b>1.01</b>	<i>0.000210</i>	<i>0.117</i>
MLP	<b>79.5</b>	290.0	0.000714	0.397
Delaunay	<i>20.5</i>	3.12	3.71	2070.0
ShepMod	0.1	<i>1.45</i>	0.000220	0.122
LSHEP	0.0	3.47	<b>0.000176</b>	<b>0.0981</b>
Voronoi	0.0	3.32	0.0950	52.8
BoxSpline	0.0	1.66	0.000956	0.532

**Table 10** The left above shows how often each algorithm had the lowest absolute error approximating credit card transaction data in Table 9. On the right columns are median fit time of 5006 points, median time for one approximation, and median time approximating 556 points.

Algorithm	Min	25 <sup>th</sup>	50 <sup>th</sup>	75 <sup>th</sup>	Max
Delaunay	<b>0.0287</b>	<b>0.0914</b>	<b>0.158</b>	<i>0.308</i>	<i>0.897</i>
ShepMod	0.0307	<i>0.0983</i>	<i>0.164</i>	0.335	1.0
Voronoi	<i>0.0303</i>	0.1	0.165	<b>0.274</b>	<b>0.762</b>
BoxSpline	0.0679	0.429	0.571	0.752	1.0

**Table 11** This numerical data accompanies the visual provided in Figure 13. The columns of absolute error percentiles correspond to the minimum, first quartile, median, third quartile, and maximum KS statistics respectively between truth and guess for models predicting the distribution of I/O throughput that will be observed at previously unseen system configurations. The minimum value of each column is boldface, while the second lowest is italicized. All values are rounded to three significant digits.

Algorithm	% Best	Fit/Prep. Time (s)	App. Time (s)	Total App. Time (s)
Delaunay	<b>62.0</b>	0.344	0.00984	2.71
ShepMod	0.0	<b>0.0884</b>	<b>0.000145</b>	<b>0.0436</b>
Voronoi	<i>38.0</i>	0.360	0.00253	0.762
BoxSpline	0.0	<i>0.0972</i>	<i>0.000210</i>	<i>0.0633</i>

**Table 12** The left above shows how often each algorithm had the lowest KS statistic on the I/O throughput distribution data in Table 11. On the right columns are median fit time of 2715 points, median time for one approximation, and median time approximating 301 points.